Reliability of Linear WSNs: A Complementary Overview and Analysis of Impact of Cascaded Failures on Network Lifetime*

Muhammed Fatih Carsancakli[a], Md Abdullah Al Imran[b], Huseyin Ugur Yildiz[c,*], Ali Kara[d], Bulent Tavli[a]

[a]*Department of Electrical and Electronics Engineering, TOBB University of Economics and Technology, Ankara, 06560, Turkey*
[b]*Department of Electrical and Electronics Engineering, Atilim University, Ankara, 06830, Turkey*
[c]*Department of Electrical and Electronics Engineering, TED University, Ankara, 06420, Turkey*
[d]*Department of Electrical and Electronics Engineering, Gazi University, Ankara, 06570, Turkey*

Abstract

Linear Wireless Sensor Networks (LWSNs) are used in applications where deployment scenarios necessitate sensor nodes to be placed over a line topology. However, such a deployment raises reliability concerns because almost all the nodes in the network are critical with respect to the survivability of the LWSN. It is possible that an LWSN can stay connected even if a subset of the nodes are eliminated, yet, the potential reduction in Network Lifetime (NL) due to such an occurrence can be significant. In this study, after presenting a concise survey of the literature on LWSN reliability, we present an elaborate optimization framework to model the operation of an LWSN, which is built upon a comprehensive system model. Our framework encom-

*This work is partially funded by TUBITAK (The Scientific and Technological Research Council of Turkey) under Project Number 5160097 and Kortek Corrosion Technologies Co. Ltd.

*Corresponding Author

Email addresses: mcarsancakli@etu.edu.tr (Muhammed Fatih Carsancakli), alimran.abdullahmd@student.atilim.edu.tr (Md Abdullah Al Imran), hugur.yildiz@tedu.edu.tr (Huseyin Ugur Yildiz), akara@gazi.edu.tr (Ali Kara), btavli@etu.edu.tr (Bulent Tavli)

passes three transmission power and packet size assignment strategies, which are instrumental in characterizing LWSN behavior. Furthermore, we utilized two-node failure models (i.e., random and coordinated) to assess the vulnerability of LWSNs from multiple perspectives. The results of this study reveal that the impact of coordinated node failures on NL is more severe than the impact of random node failures to such extent that in strongly connected LWSNs, the percentage decrease in NL due to coordinated node failures can be more than a magnitude higher than the NL decrease due to random node failures.

Keywords: linear wireless sensor networks, reliability, cascaded failures, network lifetime optimization, data packet size, transmission power level

---

1. Introduction

The vision for employing a system comprised of networked sensing devices, which are currently known as Wireless Sensor Networks (WSNs), for monitoring and surveillance of a predetermined geographic area has been utilized for more than half a century. Indeed, the armed forces of the USA have experimented with an early version of WSNs during the Vietnam conflict (i.e., Operation Igloo White) [1]. However, the most intense phase of research and development on WSNs has begun at the dawn of the third millennium [2]. Since then, WSN technology has taken a rapid pace, and currently, deployment of WSNs for a wide range of use cases is a common occurrence [3, 4, 5].

Among many deployment scenarios and topologies, linear topology WSN deployments (i.e., the network is not linear, but the topology is) constitute a particularly important type of WSNs, known as Linear WSNs (LWSNs) [6]. In fact, LWSNs have a wide range of application areas, such as monitoring and surveillance for oil, gas, and water pipelines [7]. An analysis of the most fatal oil and gas pipeline accidents in history has revealed that a critical portion of such accidents could have been prevented by proper monitoring of the pipelines [8] (perhaps through the deployment of LWSNs). Border surveillance, railroad monitoring, and historic site monitoring are also among the application areas of LWSNs [9]. Although for most of these deployments, LWSNs do not strictly form straight lines along with the whole deployment, in a significant portion of the deployment, sensor nodes are deployed, at least, roughly, along a straight line [10]. Hence, analyzing a line network, which rep-

Table 1: Symbols/Acronyms, descriptions, and values (where relevant).

Sym/Acr	Description (Value)	Sym/Acr	Description (Value)
d_{ij}	distance between node-i and node-j	ϕ_{ij}	path-loss between node-i and node-j (m)
d_0	reference distance (1 m)	ϕ_0	reference path-loss (55 dB)
X_σ	shadowing term (dB)	σ	standard deviation of the shadowing term (dB)
α	path-loss exponent	P_ω	noise power (~ -120 dBm)
P_{tx}^l	power consumption for TPL-l (mW)	$P_{tx}^{out,l}$	output power at TPL-l (dBm)
P_{rx}	power consumption for reception (69 mW)	$P_{rx,ij}^{m,l}$	received signal power at node-j (dBm)
χ_{ij}^l	SNR of the signal received at node-j (dB)	$\rho_{ij}^{l,s}(\eta)$	probability of successfully receiving an η-byte packet
$\rho_{ij}^{l,f}(\eta)$	PER	$\beta_{ij}^{lkm,s}$	two-way successful handshake probability
η	packet size (generic)	η^m	data packet size (bytes)
η_A	ACK packet size (12 bytes)	$E_{tx}^l(\eta^m)$	energy cons. for an η^m-byte packet transmission (J)
$T_{tx}(\eta^m)$	duration of transmission (s)	ζ	channel rate (250 kbps)
T_{slot}^m	time slot duration (s)	T_{grd}	guard time (100 μs)
T_{prp}	max. propagation delay (100 μs)	$E_{tx}^{HS}(\eta^m)$	transmitter's energy dissipation for a handshake (J)
λ_{ij}^{lkm}	retransmission rate	$E_{tx,ij}^{lkm}$	transmitter's average energy diss. for a handshake (J)
E_P^m	data processing energy dissip. ($E_P^m = 0.1055\eta_D^m$ μJ)	$E_{rx}^{HS,s}$	receiver's energy diss. for a successful handshake (J)
$E_{rx}^{HS,f}$	receiver energy diss. for a failed handshake (J)	$E_{rx,ji}^{lkm}$	receiver's average energy diss. for a handshake (J)
V	set of all nodes	W	set of sensor nodes
G	graph representation of the network	(i,j)	link from node-i to node-j
A	set of links (arcs)	f_{ij}^{lkm}	number of packets flowing from node-i to node-j
S_L	TPL set	S_M	DPS set ($S_M = \{28, 32, 38, 48, 68, 128\}$ bytes)
N_{rnd}	number of rounds	T_{rnd}	round duration (20 s)
s_i	data generated at each round (120 bytes)	η_D^m	payload size of a data packet (bytes)
η_H	header size of a data packet (8 bytes)	T_{DA}	time spent for data acquisition at each round (5 ms)
T_{busy}^n	total time spent when not in sleep mode (s)	P_{slp}	power consumption in sleep mode (3 μW)
E_{DA}	data acquisition energy (57 μJ)	e_i	initial battery energy of each sensor node (15 kJ)
I_{jnlk}^i	interference matrix	P_ν	interference threshold (~-125 dBm)
a_{lkm}	binary indicator variable used for NetPS	M	a large number
l_{ij}	optimal data TPL on link (i,j) for LnkPS	k_{ji}	optimal ACK TPL on link (j,i) for LnkPS
m_{ij}	optimal DPS on link (i,j) for LnkPS	γ	size of the set of failed nodes
LWSN	linear wireless sensor network	QoS	quality-of-service
NL	network lifetime	TPL	transmission power level
DPS	data packet size	ACK	acknowledgment (packet or operation)
PE	propagation environment	LnkPS	link-level TPL and DPS optimization strategy
NetPS	network-level TPL and DPS optimization strategy	FixPS	highest TPL and lowest DPS assignment strategy
RNF	random node failure model	CNF	coordinated node failure model
MIP	mixed integer programming	IND	inter-node distance
SNR	signal-to-noise ratio	PER	packet error rate

resents an LWSN deployment, is a sensible and plausible approach. For the convenience of the reader, notations/symbols/acronyms we use throughout the paper, along with the parameter values, where applicable, are presented in Table 1.

One of the most important Quality-of-Service (QoS) metrics for WSNs is Network Lifetime (NL) [11, 12, 13]. In fact, maximizing NL has been the most intensively investigated performance metric in WSN literature [14, 15, 16]. Transmission Power level (TPL) assignment and Data Packet Size (DPS) assignment are two effective means to reduce the energy waste in WSNs [17, 18, 19, 20, 21] (among others). The objective in TPL assignment is to assign the optimal TPL to a transmitter so that either utilizing an unnecessarily high TPL on a low path-loss channel or employing an inadequately low TPL on a high path-loss channel are both avoided [22, 20]. By the same token, using a lower DPS on a high path-loss channel reduces

the probability of retransmissions, while utilizing a higher DPS on a low path-loss channel is generally preferable [19]. Joint optimization of TPL and DPS is an approach that significantly prolongs NL [23]. Furthermore, there are two general joint optimization categories: (i) network-level and (ii) link-level. In the network-level approach, a single optimized TPL and a single optimized DPS are adopted throughout the network on all links, whereas, in the link-level approach, optimal TPL and DPS are determined for each link in the network individually. Although the network-level approach is more convenient than the link-level approach from an operational point of view, the link-level approach has the potential to avoid energy waste that can be introduced by the network-level approach. Nevertheless, the efficiency of joint optimization strategies is dependent on the network topology as well as the propagation environment, among other factors [24].

It can be argued that recharging or replacing the batteries of sensor nodes can be a viable alternative to extend the network lifetime for some applications of LWSNs. However, in some other applications of LWSNs powering the sensor nodes by batteries has certain advantages also. For example, considerably long segments of gas pipelines are deployed over terrains (e.g., mountain ranges) that are not accessible during the winter months due to harsh weather conditions. Therefore, replacing the batteries in such deployments of LWSNs is not possible or extremely challenging for considerably long time periods.

Reliability assessment of WSNs is as essential as providing QoS, especially for WSNs utilized to monitor critical infrastructures such as natural gas or oil pipelines [25]. In fact, large-scale LWSN deployments are frequently employed for critical or strategic infrastructure monitoring and surveillance [26]. The definition of a reliable LWSN varies according to the objective [27, 28, 29]; however, connectivity, arguably, is the most fundamental reliability metric.

It can be argued that the extent of NL decrease due to a small set of randomly selected nodes is not too high, on average; however, the reduction of NL by a specifically selected set of critical nodes can be disproportionately high [30, 31]. Nevertheless, a holistic analysis of LWSN reliability for both network-level and link-level joint TPL and DPS optimization strategies is necessary for sufficient characterization of overall system behavior. For this purpose, we adopted a Mixed Integer Programming (MIP) approach to determine the maximum NL of the LWSN under consideration [32]. Furthermore, we adopted two different strategies to model cascaded random node

failures and coordinated node failures. Both of the aforementioned strategies are utilized in conjunction with the MIP model. We adopted three Propagation Environments (PE) based on actual field measurements to model various path-loss conditions [33]. The physical layer model, which we built our models upon, is adapted from a commonly employed WSN platform [34].

Our main contributions in this study are fourfold:

1. To give a broad perspective, we present a concise and focused survey of the literature on all dimensions of our work.
2. We present three TPL and DPS assignment strategies to characterize the NL of LWSNs. Joint optimization of TPL and DPS for NL maximization in LWSNs has never been reported in the literature.
3. To assess the reliability of LWSNs operating under optimal conditions from the NL maximization perspective, we present two different node failure models (i.e., random and coordinated failures), which is also one of our novel contributions.
4. We performed extensive analysis spanning a large parameter space through numerical evaluations of the MIP models to characterize the reliability of LWSNs employing three TPL and DPS optimization/assignment strategies subject to two-node failure models and three PEs.

The rest of the paper is organized as follows. A concise survey of the related literature is provided in Section 2. Readers familiar with the topics surveyed in Section 2 can skip the first four subsections and read subsection 2.5, where we state the differences of our study from the existing literature. The system model is presented in Section 3. The results of our analyses are given in Section 4. Conclusions of this study are drawn in Section 5.

2. A Concise Overview of the Literature

There are four partially overlapping axes of the literature that we need to review to distinguish our work from the rest of the related studies in the literature. In subsection 2.1, we provide a review of LWSNs. In subsection 2.2, we present an overview of LWSN reliability. In subsection 2.3, we explore the situations, which result in premature depletion of node energy in WSNs. In subsection 2.4, we explore the literature on TPL and/or DPS assignment strategies. The novelty of our work compared to the existing literature and the gap in the literature that we fill with this study are highlighted in subsection 2.5. There are many survey/review papers on all axes of the review

we present in this section [33, 3, 4, 14, 32, 26, 35, 25, 6, 10, 7, 9, 18]. Therefore, this overview section is not intended as an alternative to the existing survey/review papers. Instead, our objective is to present the studies in the literature, which are most related to our study. We also include the most recent studies, which are not covered in other survey/review papers. Therefore, this section is intended to complement the existing survey/review papers in the literature. Furthermore, the overview presented in this section is not created as a comprehensive survey/overview of the literature.

2.1. LWSNs

There are various survey/overview papers on LWSNs in literature [36, 37, 6, 10, 7, 9]. In [36], a qualitative comparative assessment of various aspects of LWSNs for pipeline infrastructure is presented. A conceptual design framework for LWSNs which can be utilized for monitoring the critical and essential infrastructures of pipelines carrying oil, gas, and water is also elaborated. In [37], application scenarios for LWSNs are explored, a taxonomy of LWSNs by considering topology and hierarchy aspects is provided, and future research directions are discussed. In [6], an overview of applications, requirements, and features of LWSNs is presented. Furthermore, two taxonomies based on topology and hierarchy are created. In [10], a novel taxonomy of leak detection methods is presented. Moreover, WSN-based leak detection approaches are surveyed. It is argued that WSNs, in general, and LWSNs, in particular, provide monitoring services that have significant roles in the oil and gas industry not only to preserve the process quality but also to prevent possible environmental hazards. In [7], a comprehensive survey of WSNs in the oil and gas industry is presented; which, inherently covers applications of LWSNs in certain scenarios. Requirements, taxonomy, recent advances, and open research challenges are also addressed therein in detail. In [9], an overview of routing techniques employed by LWSNs is presented using a novel taxonomy, and a comparative qualitative analysis of the routing techniques is provided.

In the rest of this subsection, we present selected prominent studies utilizing LWSNs in chronological order. In [38], the design, deployment, and experimental evaluation of a WSN architecture for pipeline monitoring (PipeNet) are presented. Indeed, this is one of the earliest (if not the earliest) experimental LWSN deployments. In [39], a routing approach (Minimum Energy Relay Routing – MERR) for minimizing total energy dissipation in LSWNs

is proposed. Both stochastic analysis and simulations reveal that the performance of MERR approaches theoretical bounds. In [40], an approach for node placement in LWSNs is presented. The goal is to make each node dissipate the same amount of energy at each data collection period, which is shown to prolong NL significantly. Energy dissipation characteristics with random node placement are also investigated. In [41], an analysis framework is presented for the characterization of load distribution over an LWSN by considering the number of nodes and their spatial distribution. In [42], a WSN that detects, identifies and localizes problems in pipelines in oilfields (SWATS) is presented, which is similar in nature to PipeNet. The most important advantage of SWATS is that it can perform in-network processing to make inferences based on multi-modal sensing and multi-sensor collaboration. In [43], an optimization strategy to prolong NL of LWSNs via a mobile sink is proposed, which is shown to elongate NL significantly compared to the NL of static LWSNs.

In [44], a complete LWSN architecture encompassing the platform design (i.e., the SimpliMote), networking architecture, data processing block, and information extraction stage are designed and implemented. Performance evaluations through direct experimentation reveal that the mission-intensive SimpliMote platform outperforms a well-known generic platform (i.e., Arduino) in terms of energy efficiency, reliability, and timeliness. In [45], an LWSN-based monitoring system for cathodic protection (i.e., protection against corrosion) of oil and natural gas pipelines are proposed. In [46], an interference analysis model for LWSNs, which employ duty-cycling and pipelined-forwarding protocol, is presented. The model is shown to be instrumental in providing guidelines for duty cycle setting to attain the desired performance level. In [47], a Lyapunov-based algorithm that minimizes packet dropping probability for energy harvesting LWSNs under data queue stability and quality of monitoring constraints is proposed.

In [48], an integrated local synchronization and relaying approach for LWSNs is proposed, and its performance is evaluated through simulations. In [49], a comparative evaluation of LWSN energy minimization through optimal node placement and equidistant node placement strategies is presented. In [50], an LWSN-based water quality monitoring system is proposed. In [51], an optimal energy allocation approach for LWSNs to monitor intelligent railway systems is proposed. In [52], a modified lion optimization algorithm is proposed to boost the performance of LWSNs in terms of delay, throughput, and NL. In [53], the impact of synchronization window and offset/drift mode

selection on the performance of LWSNs are explored through direct experimentation. In [54], the use of implicit confirmation (iACK) in LWSNs to optimize energy dissipation and delay is analyzed.

2.2. LWSN Reliability

The reliability of LWSNs is a particularly important issue due to the specific topology of the network, which renders the network extremely vulnerable to failures [55]. In this subsection, we overview representative studies on LWSN reliability.

In [28], the impact of the failure of a plurality of contiguous nodes on the sensing loss in LWSNs is investigated. An analytical model for estimating sensing loss is created and analyzed under various network and fault scenarios. In [29], an analytical model for providing reliability analysis of LWSNs is proposed. The model is employed in the creation of periodic maintenance schedules and in designing robust LWSN structures. In [56], a range of node failures in LWSNs and their impact on coverage is investigated through an analytical model. In [57], an analysis framework is presented to rank the nodes according to their impact on LWSN reliability and identify the most critical LWSN node to improve network reliability. In [27], an Internet-of-Things (IoT)-based LWSN architecture is proposed to make data collection as convenient, rapid, robust, and reliable as possible. In [58, 59], a multi-valued decision diagram-based analytical model is created and evaluated for LWSNs incorporating backbone nodes. More specifically, the efficiency of the model is demonstrated in the creation of an optimal backbone node allocation strategy. In [60], comparative evaluations of six LWSN scenarios based on LoRaWAN are presented to detect black powder in pipelines from reliability and availability perspectives.

2.3. Abnormal Energy Depletion in WSNs

NL is one of the most important performance metrics of WSNs. Indeed, awareness of the reasons for premature reduction of WSN NL is a vital reliability concern. In this subsection, we present an overview of the literature on various threats against WSNs with a target of abnormal NL reduction. The lessons learned from such cases are invaluable in LWSN reliability assessment.

In [61], vampire attacks are defined, which rapidly drain battery energies of nodes, thereby distracting data flow within the network. In fact, such attacks are shown to be devastating and challenging to detect yet can be conveniently performed. In [30], the impact of eliminating the most critical

node on NL of WSNs is investigated. In [62], a novel battery depletion attack against WSNs (i.e., denial-of-battery attack) is identified and explored through a mathematical model based on random processes. In [63], a battery exhaustion attack, which attains abnormal drainage of battery energy by exploiting Constrained Application Protocol (CoAP), is experimentally demonstrated. In [31], the impact of coordinated multiple critical node failures on NL of WSNs is investigated. In [64], a survey of attacks targeting energy provisioning in WSNs is presented, and the effects of such attacks on NL are investigated. Furthermore, a novel countermeasure against these attacks is proposed and evaluated.

In [65], an approach for proactively identifying critical nodes in a network and installing backup nodes to mitigate the effects of eliminating identified critical nodes is proposed. In [35], a survey of power analysis attacks in WSNs is presented. In [66], an efficient detection and isolation mechanism against various attacks, including denial-of-sleep attacks, is presented. Jamming mechanisms can be used to perform denial-of-sleep, especially in time-synchronized and channel hopping enabled networks. In [67], jamming attacks against IoT networks for preventing communications is investigated. In [68], a systematic overview of energy depletion attacks against the energy-constrained devices in IoT networks is presented. In [69], an efficient mechanism to counter the energy depletion attacks in wireless networks, where communication and power transfer occurs simultaneously, is proposed. The burden of providing energy is designated to be the responsibility of the entity making the networking requests (i.e., power-positive networking). In [70], two novel reliability metrics are introduced for overall reliability and instantaneous reliability in WSNs. Furthermore, an efficient design methodology with three stages is proposed to improve reliability.

2.4. TPL and/or DPS Assignment in WSNs

The literature on TPL and/or DPS optimization/assignment in WSNs is extensive. Therefore, it is beyond the scope of this paper to present a comprehensive survey of these areas. We refer the interested readers to the survey papers and papers with extensive literature review content on these areas [71, 20, 23, 32, 14, 72, 19, 18, 17, 73, 74, 75, 24, 76, 77, 78, 79, 80, 81, 82, 21, 83]. However, we provide a review of recent and most related papers in this subsection.

2.4.1. Transmission Power Optimization

In [71], a lightweight algorithm for transmission power optimization (ATPC) for WSNs is proposed based on dynamic pairwise TPL adjustment. The performance of ATPC is evaluated through extensive field experiments, which confirm its efficiency and robustness. In [20], a TPL optimization framework for WSNs, which considers the reliability of both data and Acknowledgment (ACK) packets, is proposed, and various link-level and network-level optimization strategies are investigated. In [72], an optimization model for joint TPL assignment, mobility path selection, and data flow optimization for WSNs with multiple mobile base stations is proposed and evaluated. In [76], an opportunistic routing scheme for energy harvesting WSNs (ORDTP) is proposed, which accurately estimates the required TPL and dynamically configures the relay node-set. In [78], the modified fixed-step (MFS) distributed power control technique is presented, and its performance evaluation along with five other distributed power control algorithms is provided. In [77], a joint power control and routing scheme (PCOR), for energy harvesting WSNs is proposed, and the efficiency of PCOR is evaluated through simulations and experimental analysis. In [79], an adaptive radio and TPL selection system (ARTPoS) is presented, which supports multiple radio technologies at a single node and reveals the shortcomings of the one-radio-fits-all approach through testbed experiments. In [82], the design, implementation, and experimental evaluation of an adaptive and distributed TPL control and routing topology optimization mechanism (PC-RPL) is presented. It is argued in [21] that for low-power RF transceivers reducing TPL does not lead to significant energy savings, especially in large-scale WSNs.

2.4.2. Packet Size Optimization

In [74], the role of DPS in the energy efficiency of medium access protocols in WSNs is investigated through testbed experiments, and it is confirmed that there is an intermediate DPS representing the optimal choice for balanced energy dissipation and communication reliability. In [75], the impact of DPS on throughput in network coding-enabled wireless networks is investigated, and the optimal DPS maximizing network throughput for various scenarios is derived. In [73], the optimal DPS and inter-node distance to maximize NL in WSNs utilized for the smart grid are investigated through an optimization formulation. In [80], an experimental study for investigating the effects of DPS under controlled interference on reliability and energy efficiency of WSNs is presented, and the tradeoff between energy efficiency and robust-

ness is unearthed through an extensive set of testbed experiments. In [81], comparative evaluations of a reactive and a proactive routing protocol for different DPSs are presented.

2.4.3. Joint TPL and DPS Optimization

In [23], an optimization model based on an empirically verified characteristic of Mica2 motes is constructed to analyze the impact of TPL and DPS optimization on NL of WSNs. In [19], a joint optimization framework considering TPL and DPS in WSNs utilized for monitoring smart grid is presented. In [17], an optimization model for NL maximization by joint consideration of TPL and DPS in underwater acoustic sensor networks is proposed, and the tradeoffs involving TPL and DPS are investigated. In [24], joint optimization of DPS and TPL for each link in WSNs is explored, and nine TPL/DPS assignment strategies are comparatively evaluated. In [83], the tradeoff between energy efficiency and reliability in low-power wireless networks is investigated through a multi-objective optimization framework, where the decision space consists of DPS, the maximum number of retransmissions, and TPL.

2.5. Original contributions of this study

The closest studies in the literature to this study are [30, 31]. In [30], the impact of the failure of a randomly selected node on NL is investigated, which is extended in [31] to the failures of multiple nodes according to random and coordinated node failure models. However, in neither of these studies, the effects of node failures on LWSN NL are explored. Furthermore, path-loss models and energy dissipation models utilized in these studies are not as realistic as the ones employed in this study. For example, in these studies, perfect disk-shaped transmission ranges are assumed whereas in this study we utilized an empirically verified path-loss model. Moreover, data packet size and transmission power level assignment strategies we investigate in this study are not considered in [30, 31].

As the aforementioned literature survey revealed, many aspects of LWSNs regarding reliability and system optimization have already been investigated. However, the reliability of LWSNs utilizing TPL and DPS optimization under cascaded random and coordinated node failures has never been investigated systematically in the literature from the perspective of NL maximization, which, considering the particularly vulnerable topology of LWSNs, is an important problem and comprehensively addressed in this study.

3. System Model

We present our system model in this section, which is inspired by and built upon many studies in the literature [22, 24, 23, 17, 19, 72, 20, 83, 31, 30, 84, 11, 33], yet, it is a refined and unique synthesis, carefully tailored to facilitate a clear assessment of the research problems investigated in this study.

3.1. Overview

The main pillars of the system model are as follows

1. To be able to perform a realistic assessment of LWSN NL, we adopted empirically verified path-loss models, which are presented in subsection 3.2.
2. We adopted the characteristics of an existing and widely employed sensor node platform, which is introduced in subsection 3.3.
3. We created a detailed energy dissipation model based on the aforementioned path-loss model and sensor node platform, elaborated in subsection 3.4.
4. To characterize the performances of network-level, link-level, and topology-insensitive TPL and DPS assignment strategies, we designed three optimization models, which are explained in subsection 3.5.
5. To assess the effects of node failures on LWSN NL, we introduced two cascaded node failure models (random and coordinated), which are provided in subsection 3.6.
6. The system model is based on realistic assumptions and reasonable abstractions; therefore, the performance evaluations we present in this study reveal the best system behavior under idealized yet, realistic operation conditions.
7. The system model is created to characterize the system behavior but not to propose a new algorithm/approach to prolong the LWSN NL or reliability. Therefore, comparisons with any heuristic models, potentially leading to sub-optimal solutions, are not meaningful when the optimal results are readily available. Hence, the contributions of this study do not include the creation of a new algorithm/technique; instead, the contributions are due to the creation of the system model and the characterization of LWSN reliability (in terms of NL) by using the system model under optimal operating conditions.

We considered an LWSN consisting of a plurality of sensor nodes and a base station (sink) located at one end of the network. Sensor nodes are placed along with a line topology equidistantly; however, path-loss values can be (and most probably are) different due to the statistical nature of the path-loss model adopted. The LWSN is orchestrated by the base station as the central controller. All the nodes in the LWSN are time-synchronized, which enables the nodes to organize the time into constant duration rounds. We also have guard times (T_{grd}) in time slots to ease the synchronization requirements. We assume a TDMA (Time Division Multiple Access) scheme is in effect. Each sensor node creates the same amount of data at each round and conveys packetized data towards the sink, either directly or through other sensor nodes acting as relays. The objective is to maximize LWSN NL by optimizing data flow and energy dissipation patterns of sensor nodes to prevent any sensor node from dissipating its battery energy inefficiently.

3.2. Path-Loss Model

We consider a near-ground PE. It is shown that the log-normal shadowing path-loss model is appropriate for such an environment through direct experimentation [33]. Path-loss between node-i and node-j (separated by a distance d_{ij}) is denoted by ϕ_{ij} and can be calculated (in dB) using the log-normal shadowing model as follows

$$\phi_{ij} = \phi_0 + 10\alpha \log_{10}\left(\frac{d_{ij}}{d_0}\right) + X_\sigma, \tag{1}$$

where ϕ_0 is the reference path-loss at the reference distance d_0 , α is the path-loss exponent, X_σ models the shadowing phenomena, which is a Gaussian random variable with $\mathcal{N}(0, \sigma)$ distribution, and the total noise power is denoted by P_ω. We utilized three PEs with parameters given in Table 2 [33]. Note that in the ascending order, the PEs get harsher. For example, Propagation Environment 1 (PE1) is the mildest environment, and PE3 is the harshest environment. The parameters, α and σ, depend on the environment, and they are obtained using empirical analysis.

3.3. Transceiver Model

We adopt the energy dissipation characteristics of the Tmote Sky platform equipped with Chipcon CC2420 transceivers [34]. Eight different power levels (`PA_LEVEL`) are reported for the Chipcon CC2420 transceivers (i.e.,

Table 2: Parameters of the propagation environments.

	α	σ
Propagation Environment 1	1.75	2.00
Propagation Environment 2	2.00	2.25
Propagation Environment 3	2.25	2.50

PA_LEVEL varies from 3 to 31 with an increment of 4). We assume that PA_LEVEL = 3 corresponds to the minimum TPL (i.e., $l = 1$), while PA_LEVEL = 31 corresponds to the maximum TPL (i.e., $l = 8$). The output antenna power (i.e., $P_{tx}^{out,l}$) ranges from -25 dBm to 0 dBm as l ranges from 1 to 8. Multiplying the current consumption in the transmit mode by the supply voltage of the on-chip voltage regulator (i.e., 3 V nominal) for the CC2420 radios, we calculate the circuit power consumption at each TPL-l (P_{tx}^{l}). TPLs (l), power dissipation at TPL-l (P_{tx}^{l}), and output antenna power at TPL-l ($P_{tx}^{out,l}$) are given in Table 3. The power consumption for reception (P_{rx}) is constant, which is obtained by multiplying the current consumption in the receive mode by the nominal supply voltage (i.e., 69 mW).

Table 3: TPLs (l), antenna output powers $P_{tx}^{out,l}$ (in dBm), and circuit power consumptions P_{tx}^{l} (in mW) for Tmote Sky motes.

l	P_{tx}^{l}	$P_{tx}^{out,l}$	l	P_{tx}^{l}	$P_{tx}^{out,l}$
1	25.5	-25	5	41.7	-5
2	29.7	-15	6	45.6	-3
3	33.6	-10	7	49.5	-1
4	37.5	-7	8	52.2	0

3.4. Energy Dissipation Model

The received signal power at node-j due to the transmission from node-i at TPL-l (in dBm) is computed as

$$P_{rx,ij}^{in,l} = P_{tx}^{out,l} - \phi_{ij}. \tag{2}$$

The signal-to-noise ratio (SNR) of the signal received at node-j due to the transmission of node-i at TPL-l (in dB) is

$$\chi_{ij}^{l} = P_{rx,ij}^{in,l} - P_{\omega}. \tag{3}$$

Chipcon CC2420 transceivers use O-QPSK (offset-quadrature phase-shift keying) for modulation. For this modulation technique, the probability of receiving a packet of size η bytes without any errors is

$$\rho_{ij}^{l,s}(\eta) = \left(1 - Q\left(\sqrt{\frac{2E_b}{N_0}}\right)\right)^{8\eta}, \tag{4}$$

where $Q(.)$ is the tail distribution function of the standard normal distribution, $\frac{E_b}{N_0} = G_P 10^{(0.1\times\chi_{ij}^l)}$ is the SNR per bit, and $G_P = 8$ is the processing gain of the Tmote Sky node platform [19]. The packet error rate (PER) can be expressed as

$$\rho_{ij}^{l,f}(\eta) = 1 - \rho_{ij}^{l,s}(\eta). \tag{5}$$

In practical wireless communications systems, data exchange occurs through handshaking (i.e., data packet receptions are acknowledged by ACK packets). If an ACK packet is not received after a predetermined time (i.e., a timeout occurs), then the handshake is assumed to be failed. The two-way successful handshake probability, $\beta_{ij}^{lkm,s}$, for an η^m-byte data packet transmitted at TPL-l and an η_A-byte ACK packet transmitted at TPL-k is obtained by multiplying successful reception probabilities of both data and ACK packets as

$$\beta_{ij}^{lkm,s} = \rho_{ij}^{l,s}(\eta^m)\rho_{ji}^{k,s}(\eta_A). \tag{6}$$

Energy consumption for transmission of an η^m-byte packet at TPL-l is computed as

$$E_{tx}^l(\eta^m) = P_{tx}^l T_{tx}(\eta^m), \tag{7}$$

where $T_{tx}(\eta^m)$ is the duration of an η^m-byte packet transmission and calculated by dividing the packet size to the channel data rate, ζ.

After an η^m-byte packet transmission, the transmitting node-i waits in the reception mode for a duration of $T_{slot}^m - T_{tx}(\eta^m)$ until the end of the time slot allocated for the handshake, which has a duration of T_{slot}^m. The duration of a time slot is

$$T_{slot}^m = 2T_{grd} + T_{tx}(\eta^m) + T_{prp} + T_{tx}(\eta_A), \tag{8}$$

where T_{prp} and T_{grd} denote the round-trip propagation delay and the guard time (for preventing synchronization errors), respectively. The energy dissipation of a data transmitting node is the same whether the ACK packet is received successfully or not. Hence, the energy dissipation of the data transmitting node for a successful handshake is

$$E_{tx}^{HS}(\eta^m) = E_{tx}^{l}(\eta^m) + P_{rx}(T_{slot}^{m} - T_{tx}(\eta^m)), \tag{9}$$

where $E_{tx}^{l}(\eta^m)$ and $P_{rx}(T_{slot}^{m} - T_{tx}(\eta^m))$ are the energy consumed in the transmission mode and the reception mode, respectively.

Due to the error-prone nature of the wireless channel, we assume a retransmission scheme is in effect. On the average, a handshake operation has a retransmission rate of

$$\lambda_{ij}^{lkm} = \frac{1}{\beta_{ij}^{lkm,s}}. \tag{10}$$

In other words, λ_{ij}^{lkm} is the average number of transmissions for ensuring that an η^m-byte packet is successfully received at the receiver node-j. Hence, the average energy dissipation of a data transmitting node for a handshake, including the energy dissipation for retransmissions, is

$$E_{tx,ij}^{lkm} = E_{P}^{m} + \lambda_{ij}^{lkm} E_{tx}^{HS,l}(\eta^m), \tag{11}$$

where E_{P}^{m} is the energy dissipation for data processing.

The energy dissipation of the intended recipient of a data transmission (node-j) for a successful handshake is due to the reception of data packet, which costs of $P_{rx}(T_{slot}^{m} - T_{tx}(\eta_A))$ energy, and the transmission of ACK packet, which requires of $E_{tx}^{k}(\eta_A)$ energy. Therefore, the energy consumed at the receiver during a successful handshake is expressed as follows

$$E_{rx}^{HS,s}(\eta_A) = E_{tx}^{k}(\eta_A) + P_{rx}(T_{slot}^{m} - T_{tx}(\eta_A)), \tag{12}$$

As long as the data packet is received successfully by node-j, the energy expenditure of node-j does not change even if node-i cannot receive the ACK packet successfully. However, if node-j cannot receive the data packet successfully, the receiver node-j would stay in the receiver node for the whole slot duration. In this case, the energy expenditure of node-j becomes

$$E_{rx}^{HS,f} = P_{rx} T_{slot}^{m}. \tag{13}$$

Therefore, taking the retransmissions into account, the average energy spent at the data receiving node for handshaking is

$$E_{rx,ji}^{lkm} = E_P^m + \lambda_{ij}^{lkm} \Big[\beta_{ij}^{lkm,s} E_{rx}^{HS,s}(\eta_A) + \rho_{ij}^{l,s}(\eta^m) \rho_{ji}^{k,f}(\eta_A) E_{rx}^{HS,s}(\eta_A) + \rho_{ij}^{l,f}(\eta^m) E_{rx}^{HS,f} \Big]. \quad (14)$$

Note that the term $\lambda_{ij}^{lkm} \rho_{ij}^{l,s}(\eta^m) \rho_{ji}^{k,f}(\eta_A)$ accounts for the failed handshake case due to the failure of an ACK packet (i.e., the case where a data packet is successfully received but the ACK packet fails in the reverse direction).

3.5. Optimization Model

We construct an optimization framework to model three TPL and DPS assignment strategies. In the Link-level TPL and DPS Optimization (LnkPS) strategy, data and ACK TPLs and DPSs are optimized for all links. In the Network-level TPL and DPS Optimization (NetPS) strategy, a single set of optimal data/ACK TPLs and DPS is utilized for all links throughout the network. In the Fixed highest TPL and lowest DPS assignment (FixPS) strategy, the highest TPL and the lowest DPS are utilized independently of the network topology. In fact, these three strategies can be considered as the generalized abstractions of design ideas employed by TPL and/or DPS optimization approaches proposed in the literature [11, 84, 71, 20, 23, 72, 19, 30, 31, 17, 78, 24, 79, 46, 73, 74, 75, 80].

We use a graph-theoretical abstraction to model an LWSN, where the network is modeled as a directed graph $G(V, A)$. The set of nodes are denoted by set V, and the set of links are denoted by set $A = \{(i, j) : i \in V, j \in V - i\}$. For ease of exposition, we define another set, W, which is the set of sensor nodes only. The set of TPLs is defined in subsection 3.3 and denoted by S_L. The set of DPSs is denoted by S_M.

3.5.1. Generic Optimization Model

We, first, present a generic optimization model. Later we built the optimization models of the other strategies upon the generic model. As stated in subsection 3.1, the time is organized into cyclic rounds. Therefore, NL can be measured in terms of the number of rounds, N_{rnd}, with the duration T_{rnd}. The generic optimization model aims to determine the optimal TPLs for data/ACK packets and DPSs utilized on each link and routing paths from sensor nodes to the base station such that the NL is maximized. Moreover,

the generic optimization model also prevents the premature death of any sensor nodes by enforcing all sensor nodes to exhaust their batteries nearly at the same time. The objective function is to maximize NL in terms of rounds, which can be expressed as

Maximize N_{rnd}.

Note that the objective of maximizing N_{rnd} is, actually, the embodiment of a widely adopted lifetime definition in the WSN field, which is the time from the beginning until the first node dies in terms of the number of rounds. Indeed, NL in seconds is $N_{rnd} \times T_{rnd}$, however, we do not maximize $N_{rnd} \times T_{rnd}$ because T_{rnd} is a constant and its inclusion in the objective function as a multiplicative term does not affect the solution of the optimization problem at all.

The constraints of the generic optimization model are given in Eqs. (15)–(20). The decision variables of the generic optimization model are listed as follows:

- f_{ij}^{lkm}: The amount of η^m-byte data packets flowing from node-i to node-j transmitted at TPL-l and acknowledged at TPL-k (positive integer variable).
- N_{rnd}: NL in terms of rounds (positive integer variable).
- T_{busy}^{i}: The total time spent on data acquisition, transmission, and reception during the entire NL by node-i (positive continuous variable).
- e_i: The total energy consumption of node-i during the entire NL (positive continuous variable).

Eq. (15) presents the flow conservation constraint. This constraint balances the incoming traffic (i.e., $\sum_{\substack{l,k\in S_L \\ m\in S_M \\ (j,i)\in A}} \eta_D^m f_{ji}^{lkm}$) and outgoing traffic (i.e., $\sum_{\substack{l,k\in S_L \\ m\in S_M \\ (i,j)\in A}} \eta_D^m f_{ij}^{lkm}$) at each sensor node (i.e., $\forall i \in W$) and the base station (i.e., $i = 1$), which is denoted by node-1.

$$\sum_{\substack{l,k\in S_L \\ m\in S_M \\ (i,j)\in A}} \eta_D^m f_{ij}^{lkm} - \sum_{\substack{l,k\in S_L \\ m\in S_M \\ (j,i)\in A}} \eta_D^m f_{ji}^{lkm} = \begin{cases} s_i N_{rnd}, & \forall i \in W \\ -s_i N_{rnd}|W|, & i = 1 \end{cases}. \tag{15}$$

We assume that each sensor node creates the same amount of data at each round, $s_i = 120$ bytes, which is conveyed to the base station either directly by the source node in its entirety and/or through the other sensor nodes acting as relay nodes in a multi-hop fashion. The total data generated by each sensor node-i during the entire NL is $s_i N_{rnd}$ bytes. On the other hand, the total data collected at the base station (node-1) during the entire NL is $s_i N_{rnd}|W|$ bytes, where $|W|$ denotes the size of the set W (i.e., the number of sensor nodes). η_D^m denotes the size of the payload portion of an η^m-byte data packet. In fact, we assumed that all data packets have a constant overhead portion (i.e., accounting for header, trailer, etc.), therefore, the relationship between the total packet size and the payload is

$$\eta^m = \eta_D^m + \eta_H, \ \forall m \in S_M. \tag{16}$$

η_D^m values are chosen as 20, 24, 32, 40, 60, and 120 bytes (e.g., $\eta_D^1 = 20$ bytes and $\eta_D^6 = 120$ bytes). On the other hand, the header length is $\eta_H = 8$ bytes.

Throughout the operational lifetime of an LWSN, a sensor node dissipates energy in the transmission mode, reception mode, data acquisition mode, and sleep mode. At each round each sensor node spends T_{DA} amount of time in the data acquisition mode. Thus, during the entire NL, a sensor node stays in the data acquisition mode for a duration of $N_{nrd}T_{DA}$. Any node involved in a handshake stays in the reception or transmission mode during the entire duration of the corresponding time slot. Therefore, the total busy time of node-i, T_{busy}^i, which is the total time spent on the data acquisition (i.e., $N_{rnd}T_{DA}$), transmission (i.e., $\sum_{\substack{l,k\in S_L \\ m\in S_M \\ (i,j)\in A}} T_{slot}^m \lambda_{ij}^{lkm} f_{ij}^{lkm}$), and reception (i.e., $\sum_{\substack{l,k\in S_L \\ m\in S_M \\ (j,i)\in A}} T_{slot}^m \lambda_{ji}^{lkm} f_{ji}^{lkm}$) including the effects of retransmissions during the entire NL, can be expressed in Eq. (17) as

$$T_{busy}^i = N_{rnd}T_{DA} + \sum_{\substack{l,k\in S_L \\ m\in S_M \\ (i,j)\in A}} T_{slot}^m \lambda_{ij}^{lkm} f_{ij}^{lkm} + \sum_{\substack{l,k\in S_L \\ m\in S_M \\ (j,i)\in A}} T_{slot}^m \lambda_{ji}^{lkm} f_{ji}^{lkm}, \forall i \in W. \tag{17}$$

Eq. (18) is the energy balancing constraint that provides an upper bound on the energy dissipation of each sensor node-i by the amount of energy stored

in its battery, e_i.

$$\sum_{\substack{l,k\in S_L\\ m\in S_M\\ (i,j)\in A}} E^{lkm}_{tx,ij} f^{lkm}_{ij} + \sum_{\substack{l,k\in S_L\\ m\in S_M\\ (j,i)\in A}} E^{lkm}_{rx,ji} f^{lkm}_{ji} + P_{slp}(N_{rnd}T_{rnd} - T_{bsy,i}) + N_{rnd}E_{DA} \leq e_i, \forall i \in W. \tag{18}$$

The first term in Eq. (18) gives the total energy dissipation of node-i for time slots, where it acts as the data transmitter (i.e., $\sum_{\substack{l,k\in S_L\\ m\in S_M\\ (i,j)\in A}} E^{lkm}_{tx,ij} f^{lkm}_{ij}$), whereas the second term expresses the total energy dissipation of node-i for time slots, where it acts as the data packet recipient (i.e., $\sum_{\substack{l,k\in S_L\\ m\in S_M\\ (j,i)\in A}} E^{lkm}_{rx,ji} f^{lkm}_{ji}$). The third term accounts for the energy dissipation of node-i in the sleep mode (i.e., $P_{slp}(N_{rnd}T_{rnd} - T_{bsy,i})$), where P_{slp} denotes the power consumption in the sleep mode. The fourth term represents the energy dissipation for the data acquisition (i.e., $N_{rnd}E_{DA}$), where E_{DA} represents the average energy dissipation of each node in each round for the data acquisition.

The bandwidth usage of each node consists of the bandwidth used for the outgoing flows and incoming flows as well as the bandwidth loss incurred by the interfering flows. Eq. (19) puts an upper bound on the bandwidth usage of node-i in terms of the total capacity throughout the NL

$$\sum_{\substack{l,k\in S_L\\ m\in S_M\\ (i,j)\in A}} \lambda^{lkm}_{ij} f^{lkm}_{ij} T^m_{slot} + \sum_{\substack{l,k\in S_L\\ m\in S_M\\ (j,i)\in A}} \lambda^{lkm}_{ji} f^{lkm}_{ji} T^m_{slot} + \sum_{\substack{l,k\in S_L\\ m\in S_M\\ (j,n)\in A}} \lambda^{lkm}_{jn} f^{lkm}_{jn} I^i_{jnlk} T^m_{slot} \leq N_{rnd}T_{rnd},\ \forall i \in V. \tag{19}$$

where I^i_{jnlk} is the interference matrix [84]. The first and the second terms in Eq. (19) (i.e., $\sum_{\substack{l,k\in S_L\\ m\in S_M\\ (i,j)\in A}} \lambda^{lkm}_{ij} f^{lkm}_{ij} T^m_{slot}$ and $\sum_{\substack{l,k\in S_L\\ m\in S_M\\ (j,i)\in A}} \lambda^{lkm}_{ji} f^{lkm}_{ji} T^m_{slot}$) accounts for time slots where node-i is the data transmitter and data receiver, respectively. The third term represents the time slots, which prevents node-i from transmitting/receiving due to the interference to/from other transmitter/receiver pairs' traffic (i.e., $\sum_{\substack{l,k\in S_L\\ m\in S_M\\ (j,n)\in A}} \lambda^{lkm}_{jn} f^{lkm}_{jn} I^i_{jnlk} T^m_{slot}$). NL (in s) is given by $N_{rnd}T_{rnd}$,

which upper bounds the total time that can be utilized by any node throughout the operational lifetime of an LWSN. The interference matrix is obtained as follows

$$I^{i}_{jnlk} = \begin{cases} 1, \text{ if } P^{in,l}_{rx,ji} \geq P_{\nu} \text{ or } P^{in,k}_{rx,ni} \geq P_{\nu} \\ 0, \text{ o.w.} \end{cases} \tag{20}$$

where P_{ν} denotes a threshold determined by considering the sensitivity level of the transceiver. In fact, $I^{i}_{jnlk} = 1$ if node-j's data transmission to node-n at TPL-l and/or node-n's ACK transmission to node-j at TPL-k results in a received power level equals to or greater than P_{ν} at node-i. In other words, if node-j's and node-n's data and ACK transmissions to each other at TPL-l and TPL-k, respectively, create enough interference for node-i, then node-i cannot transmit and receive any packets during the associated time slot, which effectively is counted as a portion of node-i's utilized capacity.

Eq. 19, guarantees that there is no congestion in the network (i.e., all the data generated at the sensor nodes reach the base station). If Eq. 19 cannot be satisfied then the optimization problem has no feasible solution. We choose the relevant parameters carefully (e.g., T_{rnd}, η, and ζ) so that congestion never occurs.

We obtain Eq. 21 by dividing both sides of the inequality in Eq. 19 by N_{rnd}

$$\begin{aligned} &\frac{1}{N_{rnd}} \sum_{\substack{l,k \in S_L \\ m \in S_M \\ (i,j) \in A}} \lambda^{lkm}_{ij} f^{lkm}_{ij} T^{m}_{slot} + \frac{1}{N_{rnd}} \sum_{\substack{l,k \in S_L \\ m \in S_M \\ (j,i) \in A}} \lambda^{lkm}_{ji} f^{lkm}_{ji} T^{m}_{slot} \\ &+ \frac{1}{N_{rnd}} \sum_{\substack{l,k \in S_L \\ m \in S_M \\ (j,n) \in A}} \lambda^{lkm}_{jn} f^{lkm}_{jn} I^{i}_{jnlk} T^{m}_{slot} \leq T_{rnd}, \ \forall i \in V, \end{aligned} \tag{21}$$

which can be satisfied if the network capacity is high enough to transport all data generated at the sensor nodes to the BS at each round, on the average. Therefore, the average delay for data packets is upper bounded by T_{rnd} (20 s).

Dropped data packets due to bit errors are retransmitted until the successful transmission is achieved as stated in Eq. 11. Therefore, no packets are lost. Hence, the average aggregate end-to-end throughput per round is $|W| \times s_i$ bytes.

494 *3.5.2. Network-level TPL and DPS optimization (NetPS) Strategy*

The NetPS strategy is designed to assign a single set of data packet TPL (l), ACK TPL (k), and DPS (η^m) in all links in the network (i.e., all nodes use the same DPS and the same data packet/ACK TPLs). Although an arbitrary set can be chosen, we opt to select the optimal set that maximizes the NL. The objective function of the NetPS optimization model is the same as the generic model, i.e., Maximize N_{rnd}, and all the constraints of the generic model are in effect, i.e., Eqs. (15)–(20). However, we need to add two more constraints to ensure that there is only one set of (l, k, m) is used throughout the network. For this purpose, we define binary indicator variables a_{lkm}. Eq. (22) states that if there is any non-zero f_{ij}^{lkm} flow on any link for any particular set (l, k, m), then the binary indicator variable is set to one for this set ($a_{lkm} = 1$). The constant M is chosen to be larger than the maximum value of any f_{ij}^{lkm}.

$$\sum_{(i,j)\in A} f_{ij}^{lkm} < M \times a_{lkm},\ \forall l, k \in S_L, \forall m \in S_M. \tag{22}$$

Eq. (23) makes sure that $a_{lkm} = 1$ for only one particular set (l, k, m), which maximizes the NL when exclusively utilized for all links in the network (i.e., $f_{ij}^{lkm} \geq 0$ for only the aforementioned set and $f_{ij}^{lkm} = 0$ otherwise).

$$\sum_{\substack{l,k\in S_L \\ m\in S_M}} a_{lkm} \leq 1. \tag{23}$$

495 *3.5.3. Link-level TPL and DPS optimization (LnkPS) Strategy*

The use of the optimal (l, k, m) set for each link leads to higher NL when compared to the NetPS strategy. Therefore, in the LnkPS strategy the optimal (l_{ij}, k_{ji}, m_{ij}) set for each link is determined using Eq. (24), which minimizes the energy per byte on each link.

$$\{l_{ij}, k_{ji}, m_{ij}\} = \underset{l,k,m}{\operatorname{argmin}} \left(\frac{E_{tx,ij}^{lkm} + E_{rx,ji}^{lkm}}{\eta^m} \right),\ \forall (i, j) \in A. \tag{24}$$

496 The objective function and all the constraints of the generic optimization
497 are in effect for LnkPS optimization model, i.e., Eq. (15)–(20). However,
498 since in LnkPS, the optimal (l, k, m) set for each link is already determined
499 by Eq. (24), summations over $l, k \in S_L, m \in S_M$ are not needed any more.

Hence, all the summations are only over $(i, j) \in A$ in LnkPS model and superscripts of λ_{ij}^{lkm}, f_{ij}^{lkm}, $E_{tx,ij}^{lkm}$, $E_{rx,ji}^{lkm}$ are dropped to become λ_{ij}, f_{ij}, $E_{tx,ij}$, and $E_{rx,ji}$, respectively, i.e., the optimization model uses only the predetermined optimal (l_{ij}, k_{ji}, m_{ij}) set for each link.

3.5.4. Fixed highest TPL and lowest DPS assignment (FixPS) Strategy

The FixPs strategy is essentially the same as the NetPS strategy, such that a constant (l, k, m) set is used for all links throughout the network. However, TPLs for data and ACK packets, i.e., l, k, are chosen as the highest level provided by the transceiver employed (TPL-8, see Table 3), and DPS, i.e., m, is chosen as the lowest DPS in S_M (i.e., $\eta^1 = 28$ bytes). The FixPS strategy leads to the lowest average PER possible; however, it also wastes energy in low path-loss links by utilizing unnecessarily high TPL. Furthermore, the overhead to payload ratio is also higher than the optimal ratio for low path-loss links. Nevertheless, the FixPS strategy is instrumental in analyzing the case of over-emphasizing reliability over efficiency compared to the NetPS and LnkPS strategies. This strategy is modeled by omitting the (l, k, m) indices from the parameters and the decision variables in the generic optimization model. Furthermore, in the summations, $(l, k \in S_L)$ and $(m \in S_M)$ terms are removed from Eqs. (15)–(20)

3.6. Cascaded Node Failure Models

Node failures in WSNs, in general, and in LWSNs, in particular, can be attributed to various reasons [60, 27, 56, 28, 29, 85, 86, 87, 25, 35, 61, 30, 62, 31, 63, 64, 65, 67, 69, 68, 66, 70]. Security attacks by adversaries are one of the factors explored in the literature. Natural hazards, equipment failures, and software malfunctions (among others) can also lead to node failures. Nevertheless, we opt to explore the extent of NL reduction in LWSNs by using two generic cascaded node failure/incapacitation models without explicitly limiting the root cause to any specific factor, which facilitates a broad perspective on the reliability analysis of LWSNs. Note that for statistical significance, ensemble averaging is performed on the results obtained using both failure models.

Note that the NL definition we employed in our generic optimization model is the time from the beginning until the first node dies (i.e., the node, which dissipates the most energy determines the NL). Our target is to determine the set of critical nodes, removal of which reduces the NL most. To

achieve this target, we determine NL values in the absence of all possible sensor node sets of a predetermined size. The network topology in the absence of the most critical sensor node set results in the lowest NL. The failed nodes in our failure models do not cease to function because they consume their battery energies completely, instead, they are assumed to be incapacitated because of other reasons explained in the preceding paragraph. Therefore, we utilize the failure models to characterize the impact of the removal of a set of nodes on the remaining nodes in terms of NL. The NL definition in case of node failures is the time from the beginning until the first non-failed (i.e., not removed) node dies.

3.6.1. Random Node Failure (RNF) Model

In the RNF model, sensor nodes are removed from the graph randomly. In fact, we explore the effects of random node removal for a set of eliminated nodes, and the total number of eliminated nodes is denoted by γ. By comparing the NLs obtained through the solution of the optimization problem before and after node eliminations, the extent of the impact of node removals on LWSNs can be determined.

3.6.2. Coordinated Node Failure (CNF) Model

Unlike the random node failures model, in the CNF model, cascaded failures do not occur arbitrarily and/or independently from each other. In fact, the failed nodes are selected such that the impact of the selected node-set is the highest among all the similar size sets. Such a failure mechanism can be the result of a targeted security attack on an LWSN to decrease the NL as much as possible with a limited number of but optimally selected nodes. Another equally valid interpretation of this type of failure is that the probability of the occurrence of such a cascaded node failure is equal-likely with the occurrence probability of any other random node failure set of the same size. Therefore, the reduction in NL due to the failure of the selected nodes gives the worst-case NL reduction, hence, giving an upper bound on the extent of NL reduction.

The flowchart that outlines the operation of the coordinated node failure model is illustrated in Fig. 1. The input of the algorithm is the network graph, $G(V, A)$, and the number of nodes to be included in the failure set, γ. First, a temporary graph is created by the assignment $G_1 = G$. The inner loop runs $|W|$ times once initiated. At each run by removing each sensor node-i and the link set associated with it (A_i) from G_1 another temporary

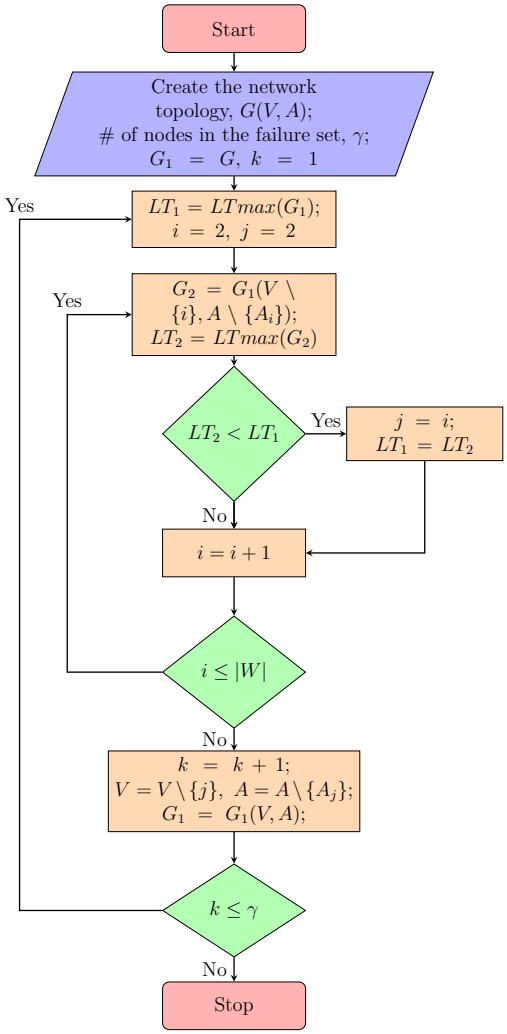

Figure 1: Sequential node elimination flowchart.

graph G_2 is created, and maximum NL computation on G_2 is performed (i.e., $LTmax(G_2)$). Upon the termination of the inner loop the node, which reduces the NL most when removed, is determined, and G_1 is updated by removing the node and all links associated with it. The outer loop executes the inner loop for γ times, and upon the termination of the outer loop, all of the γ nodes whose removal reduces the NL most are determined.

In other words, at first, using the original network topology without node failures, G, we create a temporary network topology, $G_1 = G$, and compute

the NL as $LT_1 = LTmax(G_1)$. Second, we set $k = 1$ to search for the first critical node whose failure would reduce the NL the most. To detect this node, we iterate over all the sensor nodes (i.e., $i \in W$). In each iteration, the sensor node-i is removed from the network (i.e., G_1), and corresponding links associated with the node-i (i.e., A_i) are also excluded. Hence, a new network topology without node-i and A_i is created as $G_2 = G_1(V \setminus \{i\}, A \setminus \{A_i\})$. For the new network topology, G_2, the new NL is computed and stored as $LT_2 = LTmax(G_2)$. If the new NL is greater than the original NL (i.e., $LT_2 \geq LT_1$), search for the potential node whose failure reduces the NL the most continues. On the other hand, if $LT_2 < LT_1$, the original NL is updated as $LT_1 = LT_2$, and this potential critical node whose failure would reduce the NL the most is marked (i.e., $j = i$, node-j). Third, to find the next most critical failed node (i.e., $k = 2$), G_1 is updated by excluding the previously obtained critical node (node-j) by setting $G_1 = G_1(V = V \setminus \{j\},\ A = A \setminus \{A_j\})$. Then, the same procedure to find the critical node whose failure would reduce the NL the most continues until all of the γ nodes whose removal reduces the NL the most are determined.

4. Analysis

This section systematically investigates LWSN NL through solutions of the optimization models of three TPL and DPS assignment strategies (NetPS, LnkPS, and FixPS) for three PEs, two-node failure models, and a range of Inter-Node Distance (IND) values. The system model is implemented using MATLAB and GAMS (General Algebraic Modeling System) [88]. Optimization problems are solved using the CPLEX solver. We considered LWSN deployments with 50 sensor nodes ($|W| = 50$), which are placed equidistantly (the distance between adjacent node pairs is denoted by IND), and a single base station, which is located at one end of the linear deployment. Each NL value presented is the mean of 100 random runs for statistical significance. NL values (i.e., $N_{rnd} \times T_{rnd}$) are presented in terms of years (yr), and NL values lower than 0.05 yr are treated as zero. We do not present quantitative comparisons of such data points with non-zero data points.

To assess the performances of LnkPS, NetPS, and FixPS strategies in terms of NL in three PEs and a range of INDs, we first investigate NLs without any node failures by using the data presented in Fig. 2. As the PE gets harsher, the NLs of all three strategies decrease because of the higher energy dissipation to counter the higher path-loss values. For example, NLs

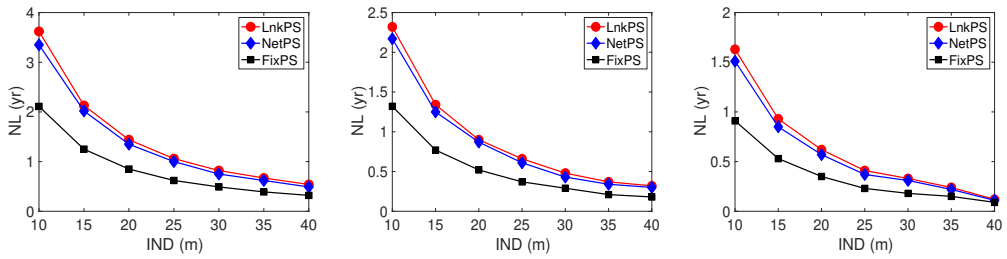

(a) PE1 (b) PE2 (c) PE3

Figure 2: NL vs. Inter-Node Distance (IND) for NetPS, LnkPS, and FixPS strategies for three propagation environments.

of LnkPS/NetPS/FixPS strategies with IND=10 m are 3.62/3.35/2.11 yr, 2.32/2.17/1.32 yr (35.80/35.24/37.30% lower than corresponding NLs in PE1), and 1.63/1.51/0.91 yr (54.85/55.02/56.73% lower than corresponding NLs in PE1) for PE1, PE2, and PE3, respectively. As IND increases, NLs for all strategies decrease in all PEs because, on average, more energy is required to transmit to farther distances. Considering the PE1, NLs of LnkPS/NetPS/FixPS strategies are 3.62/3.35/2.11 yr and 0.54/0.49/0.32 yr when IND is set to 10 m and 40 m, respectively. Nevertheless, when IND increases from 10 m to 40 m, NLs of LnkPS/NetPS/FixPS strategies decrease 85.10/85.39/84.62%, 86.26/86.02/86.77%, and 92.90/93.02/90.14%, for PE1, PE2, and PE3, respectively.

LnkPS NL values are slightly higher than NetPS NL values for all the data points because LnkPS optimizes TPL and DPS for each link, yet, NetPS utilizes a single TPL and DPS set for the whole network, which results in lower or higher than the optimal TPL and/or DPS values for some links. For instance, when IND=40 m, NLs of LnkPS and NetPS are 0.54/0.32/0.12 yr and 0.49/0.30/0.11 yr for PE1, PE2, and PE3, respectively. Nevertheless, due to the equidistant LWSN deployment, LnkPS and NetPS NLs are, fairly, close. The differences between LnkPS and NetPS NLs are within (5.39%–9.28%), (2.79%–10.42%), and (5.20%–10.32%) bands for PE1, PE2, and PE3, respectively.

NL values of both LnkPS and NetPS are significantly higher than FixPS NL values throughout the explored parameter space because of the topology insensitive TPL and DPS assignment in FixPS, which leads to significant energy waste. FixPs NLs are in the intervals of 0.32–2.11, 0.18–1.32, and 0.09–0.91 for PE1, PE2, and PE3, respectively. The differences between

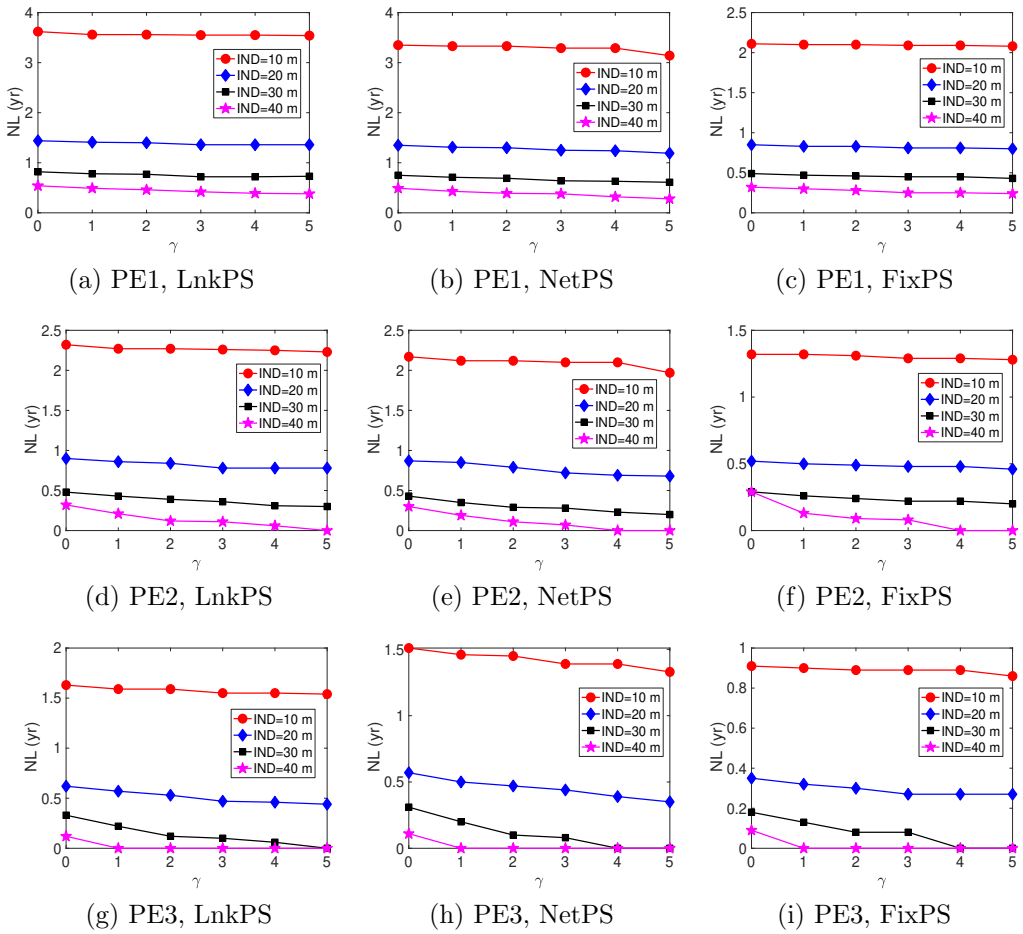

(a) PE1, LnkPS (b) PE1, NetPS (c) PE1, FixPS

(d) PE2, LnkPS (e) PE2, NetPS (f) PE2, FixPS

(g) PE3, LnkPS (h) PE3, NetPS (i) PE3, FixPS

Figure 3: NL vs. γ with RNF model for NetPS, LnkPS, and FixPS strategies for three propagation environments and INDs.

LnkPS and FixPS NL are within (39.89%–42.19%), (40.00%–45.14%), and (22.41%–46.18%) bands for PE1, PE2, and PE3, respectively.

The impact of node failures according to the RNF model is evaluated by using the data presented in Fig. 3 for three PEs, four INDs, and three strategies (LnkPS, NetPS, and FixPS) in terms of NL through varying the number of failed nodes (γ) from 0 to 5 (i.e., 10% of the total number of sensor nodes in the network, $|W|$). For all strategies, INDs, and PEs, NL decreases as γ increases, on average, because once a sensor node is incapacitated, the burden of relaying increases for the remaining sensor nodes. Indeed, failures

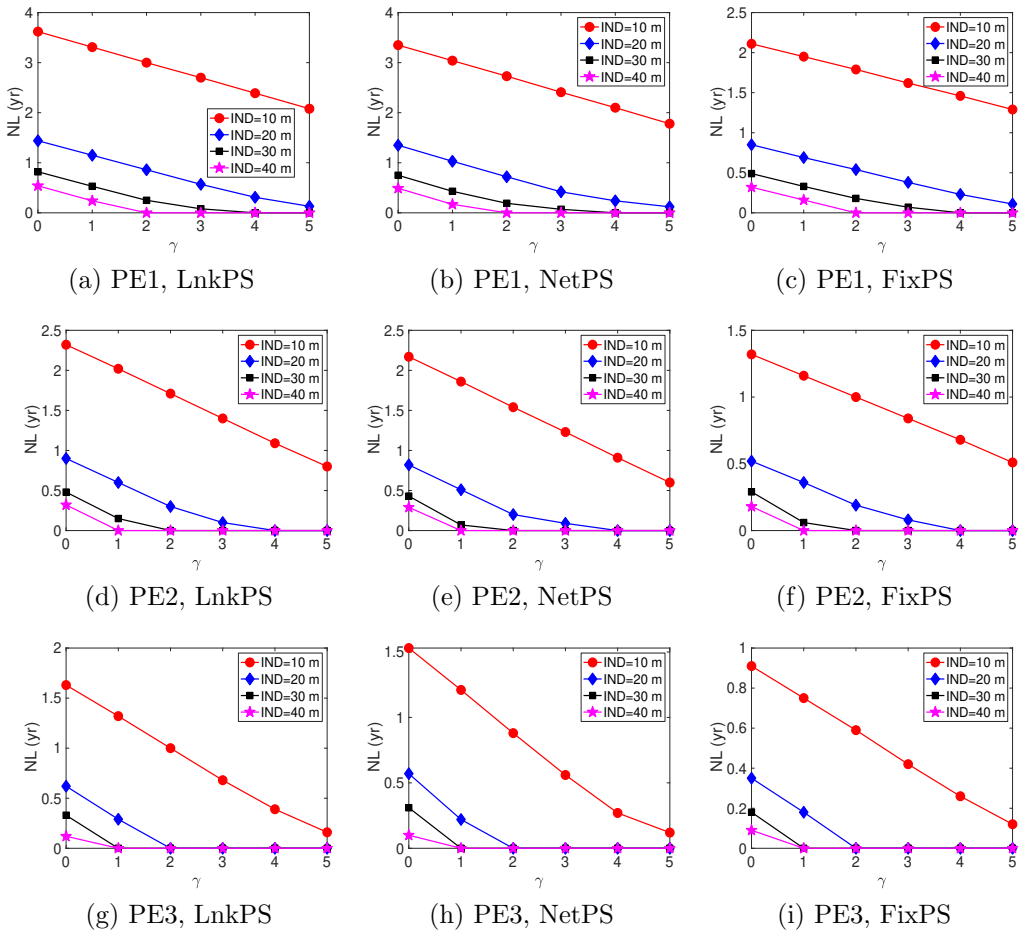

(a) PE1, LnkPS (b) PE1, NetPS (c) PE1, FixPS

(d) PE2, LnkPS (e) PE2, NetPS (f) PE2, FixPS

(g) PE3, LnkPS (h) PE3, NetPS (i) PE3, FixPS

Figure 4: NL vs. γ with CNF model for NetPS, LnkPS, and FixPS strategies for three propagation environments and INDs.

of some of the sensor nodes destroy some energy-efficient routing paths, where the failed nodes act as relays.

Throughout the parameter space explored in Fig. 3, NL of LnkPS is higher than those of both NetPS and FixPS. It is also true that NL of NetPS is always higher than or equal to that of FixPS. For example, for $\gamma \geq 1$, the difference between the NL of LnkPS and NetPS is in the range of (2.93%–32.09%), whereas the difference between the NL of LnkPS and FixPS is in the range of (21.70%–43.95%).

The decrease in NL as a function of γ is relatively lower for lower INDs.

For example, for PE1, IND=10 m, and $\gamma = 5$, NLs of LnkPS, NetPS, and FixPS decrease to 3.54 yr (2.13% decrease from NL at $\gamma = 0$), 3.14 yr (6.31%), and 2.08 yr (1.23%), respectively. However, as IND increases and PE gets harsher, the decrease in NL increases. For example, for PE2, IND=20 m, and $\gamma = 5$, NLs of LnkPS, NetPS, and FixPS decrease to 0.78 yr (12.83% decrease from NL at $\gamma = 0$), 0.68 yr (21.93%), and 0.46 yr (11.18%), respectively. In extreme cases, the decrease in NL is sharp to the point that NL approaches zero. For example, for PE3, IND=40 m, and $\gamma \geq 1$, NLs of LnkPS, NetPS, and FixPS can all be considered as zero because, in such conditions, even the removal of a single node can significantly inflate the energy cost of data transfer and nodes dissipate their limited battery energies rapidly and highly inefficiently.

To investigate the extent of the impact of node failures determined by the CNF model, we explore the data presented in Fig. 4. In general, nodes closer to the base station are selected by the CNF model, which, typically, deteriorates NL more than other possible sets of failed sensor nodes. In fact, the effects of node failures, in this case, are more severe than the case with the RNF model. Even with the mildest PE and the lowest IND, NLs of all strategies suffer very high losses. For example, for PE1, IND=10 m, and $\gamma = 5$, NLs of LnkPS, NetPS, and FixPS reduce to to 2.08 yr (42.38% decrease from NL at $\gamma = 0$), 1.78 yr (46.86%), and 1.29 yr (38.86%), respectively. Note that for PE1, IND=10 m, and $\gamma = 5$, NLs of LnkPS with the RNF and CNF models are 3.54 yr and 2.08 yr, respectively, which reveals that coordinated failures decrease NL 40% more than random failures for this scenario. In fact, IND=10 m is the only IND for which all strategies in all environments and γ values can give non-zero NLs.

For all INDs larger than 10 m, at least, for some PEs, strategies, or γ values, zero NLs are obtained. For PE2 and IND$\geq$30 m, non-zero NLs can be obtained only for $\gamma \leq 1$ for all strategies. Furthermore, none of the strategies can give a non-zero NL for PE3, IND$\geq$10 m, and $\gamma > 1$. Therefore, all the analyses show that the extent of the impact of the CNF model on NL is much more severe than the impact of the RNF model. Nevertheless, NLs obtained with LnkPS are much higher than those of NetPS and FixPS strategies. In fact, for $\gamma \geq 1$, the differences of NLs of LnkPS and NetPS are in the ranges of (8.14%–29.58%), (4.21%–33.55%), and (8.06%–31.28%), for PE1, PE2, and PE3, respectively, whereas, the differences of NLs of LnkPS and FixPS are in the ranges of (19.08%–41.08%), (35.88%–42.41%), and (27.67%–42.81%), for PE1, PE2, and PE3, respectively.

5. Conclusion

The main conclusions of this study are enumerated as follows:

1. Without considering node failures, the LnkPS strategy, which optimizes TPL and DPS for each link, results in higher NL than the NetPS strategy, which utilizes a single set of TPLs (for data and ACK packets) and a single DPS for all the links in the network (i.e., LnkPS NL is, on the average, 7.30% higher than NetPS NL and the maximum difference is 10.42%). Furthermore, NLs of both LnkPS and NetPS strategies are significantly higher than the NL of the FixPs strategy, which utilizes the highest TPL and lowest DPS on all links (i.e., LnkPS and NetPS NLs are, on the average, 41.36% and 36.68% higher than NetPS NL, respectively, and the maximum differences are 46.18% and 43.23%, respectively).
2. For random node failures case, as long as INDs are lower, and PEs are milder, even if 10% of the nodes fail, the decrease in NL is rather limited for all strategies (e.g., for IND=10 m, PE1, and $\gamma = 5$, the decrease in NLs for LnkPS, NetPS, and FixPs strategies are 2.13%, 6.31%, and 1.23%, respectively). However, for higher INDs and harsher PEs, NLs for all strategies decrease drastically as the number of failed nodes increases (e.g., NLs for all strategies approach zero for $\gamma \geq 1$, PE3, and IND=40 m). Nevertheless, the LnkPS strategy performs better than NetPS and FixPs strategies in terms of NL under random node failure scenario (i.e., NL of LnkPS is 11.28% and 37.32% higher than NetPS and FixPS strategies, respectively, on the average).
3. For all strategies, inter-node distances, and propagation environments, the impact of coordinated node failures on NL is more severe than the impact of random failures. In fact, only for the lowest IND non-zero NLs can be obtained for all strategies and in all PEs. Furthermore, the decrease in NLs due to node failures is high (e.g., for IND=10 m and $\gamma = 5$, decreases in NLs of the LnkPS strategy are 42.38%, 65.72%, 90.26%, for PE1, PE2, and PE3, respectively). Moreover, more than half of the scenarios we generated can be considered to give zero NL effectively (i.e., 91 of 180 coordinated node failure scenarios with $\gamma \geq 1$). Even under such challenging conditions performance of the LnkPS strategy in terms of NL is still higher than both NetPS and FixPS strategies (i.e., on average, LnkPS NL is 15.00% and 38.08% higher than NetPS and FixPS NLs, respectively).

4. Our results strongly suggest that under all propagation environments, inter-node distances, and a number of failed nodes, to get the best NL for LWSN deployments, it is imperative to optimize TPL and DPS for each link (e.g., LnkPS) rather than utilizing a constant TPL and DPS for all links in the network (e.g., NetPS and FixPS).
5. It is necessary to deploy LWSNs to facilitate strong connectivity (i.e., all nodes must have a sufficient number of directly reachable neighbors) to increase the resilience and reliability of the network. Such an approach, inevitably, inflates the cost of LWSN deployment (i.e., the number of sensor nodes to be deployed increases when compared to the minimum number of nodes to establish connectivity without considering node failures), yet, loss of network connectivity is a risk, which should be avoided, especially, for specific LWSN application scenarios (e.g., critical infrastructure monitoring).

References

[1] J. T. Correll, Igloo white, Air Force Mag. 87 (11) (2004) 56–61.

[2] W. B. Heinzelman, A. P. Chandrakasan, H. Balakrishnan, An application-specific protocol architecture for wireless microsensor networks, IEEE Trans. Wireless Commun. 1 (4) (2002) 660–670.

[3] L. M. Borges, F. J. Velez, A. S. Lebres, Survey on the characterization and classification of wireless sensor network applications, IEEE Commun. Surveys Tuts. 16 (4) (2014) 1860–1890.

[4] A. A. Kumar S., K. Ovsthus, L. M. Kristensen., An industrial perspective on wireless sensor networks a survey of requirements, protocols, and challenges, IEEE Commun. Surveys Tuts. 16 (3) (2014) 1391–1412.

[5] J. Wang, Y. Gao, C. Zhou, R. S. Sherratt, L. Wang, Optimal coverage multi-path scheduling scheme with multiple mobile sinks for WSNs, Computers, Materials Continua 62 (2) (2020) 695–711.

[6] S. Varshney, C. Kumar, A. Swaroop, Linear sensor networks: Applications, issues and major research trends, in: Proc. IEEE Int. Conf. Comput. Commun. Automat. (ICCCA), 2015, pp. 446–451.

[7] M. Y. Aalsalem, W. Z. Khan, W. Gharibi, M. K. Khan, Q. Arshad, Wireless sensor networks in oil and gas industry: Recent advances, taxonomy, requirements, and open challenges, J. Netw. Comput. Appl. 113 (2018) 87–97.

[8] M. Biezma, M. Andrs, D. Agudo, E. Briz, Most fatal oil & gas pipeline accidents through history: A lessons learned approach, Eng. Fail. Anal. 110 (2020) 104446:1–104446:14.

[9] S. Varshney, P. K. Rajput, A. Singh, G. Varshney, Routing techniques used for monitoring the linear structures using linear wireless sensor networks: An overview, in: Proc. Int. Conf. Comput. Commun. Intell. Syst. (ICCCIS), 2019, pp. 126–130.

[10] T. Sheltami, A. Bala, E. Shakshuki, Wireless sensor networks for leak detection in pipelines: A survey, J Ambient Intell. Human Comput. 7 (2016) 347–356.

[11] Z. Cheng, M. Perillo, W. B. Heinzelman, General network lifetime and cost models for evaluating sensor network deployment strategies, IEEE Trans. Mobile Comput. 7 (4) (2008) 484–497.

[12] J. Wang, C. Ju, Y. Gao, A. K. Sangaiah, G.-j. Kim, A PSO based energy efficient coverage control algorithm for wireless sensor networks, Comput. Mater. Con. 56 (3) (2018) 433–446.

[13] K. Vijayalakshmi, P. Anandan, Global levy flight of cuckoo search with particle swarm optimization for effective cluster head selection in wireless sensor network, Intell. Autom. Soft Comput. 26 (2) (2020) 303–311.

[14] H. Yetgin, K. T. K. Cheung, M. El-Hajjar, L. H. Hanzo, A survey of network lifetime maximization techniques in wireless sensor networks, IEEE Commun. Surveys Tuts. 19 (2) (2017) 828–854.

[15] J. Wang, Y. Gao, X. Yin, F. Li, H.-J. Kim, An enhanced PEGASIS algorithm with mobile sink support for wireless sensor networks, Wirel. Commun. Mobile Comput. 2018 (2018) 1–9.

[16] A. A. Hady, Duty cycling centralized hierarchical routing protocol with content analysis duty cycling mechanism for wireless sensor networks, Comput. Syst. Sci. Eng. 35 (5) (2020) 347–355.

[17] H. U. Yildiz, V. C. Gungor, B. Tavli, Packet size optimization for lifetime maximization in underwater acoustic sensor networks, IEEE Trans. Ind. Informat. 15 (2) (2019) 719–729.

[18] M. Yigit, S. Kurt, H. U. Yildiz, B. Tavli, V. C. Gungor, A survey on packet size optimization for terrestrial, underwater, underground, and body area sensor networks, Int. J. Commun. Syst. 31 (11) (2018) e3572:1–e3572:28.

[19] S. Kurt, H. U. Yildiz, M. Yigit, B. Tavli, V. C. Gungor, Packet size optimization in wireless sensor networks for smart grid applications, IEEE Trans. Ind. Electron. 64 (3) (2017) 23922401.

[20] H. U. Yildiz, B. Tavli, H. Yanikomeroglu, Transmission power control for link level handshaking in wireless sensor networks, IEEE Sensors J. 16 (1) (2016) 561–576.

[21] A. Pal, Transmit power reduction $\neq$ proportional power savings: Applicability of transmit power control in large-scale wireless sensor networks, IEEE Internet Things Mag. 3 (1) (2020) 20–24.

[22] M. Zuniga, B. Krishnamachari, Analyzing the transitional region in low power wireless links, in: Proc. IEEE Commun. Soc. Conf. Sens. Ad Hoc Commun. Netw. (SECON), 2004, pp. 517–526.

[23] A. Akbas, H. U. Yildiz, B. Tavli, S. Uludag, Joint optimization of transmission power level and packet size for WSN lifetime maximization, IEEE Sensors J. 16 (12) (2016) 5084–5094.

[24] H. U. Yildiz, S. Kurt, B. Tavli, Comparative analysis of transmission power level and packet size optimization strategies for WSNs, IEEE Syst. J. 13 (3) (2019) 2264–2274.

[25] Z. Zhang, A. Mehmood, L. Shu, Z. Huo, Y. Zhang, M. Mukherjee, A survey on fault diagnosis in wireless sensor networks, IEEE Access 6 (2018) 11349–11364.

[26] A. B. Noel, A. Abdaoui, T. Elfouly, M. H. Ahmed, A. Badawy, M. S. Shehata, Structural health monitoring using wireless sensor networks: A comprehensive survey, IEEE Commun. Surveys Tuts. 19 (3) (2017) 1403–1423.

[27] W. Z. Khan, M. Y. Aalsalem, M. K. Khan, M. S. Hossain, M. Atiquzzaman, A reliable internet of things based architecture for oil and gas industry, in: Proc. Int. Conf. Adv. Commun. Tech. (ICACT), 2017, pp. 705–710.

[28] N. Mohamed, J. Al-Jaroodi, I. Jawhar, S. Lazarova-Molnar, Failure impact on coverage in linear wireless sensor networks, in: Proc. Int. Symp. Perf. Eval. Comput. Telecomm. Syst. (SPECTS), 2013, pp. 188–195.

[29] N. Mohamed, J. Al-Jaroodi, I. Jawhar, A. Eid, Reliability analysis of linear wireless sensor networks, in: Proc. IEEE Int. Symp. Netw. Comput. Appl. (NCA), 2013, pp. 11–16.

[30] A. Yuksel, E. Uzun, B. Tavli, The impact of elimination of the most critical node on wireless sensor network lifetime, in: Proc. IEEE Sensors Appl. Symp. (SAS), 2015, pp. 1–5.

[31] H. U. Yildiz, B. Tavli, B. O. Kahjogh, E. Dogdu, The impact of incapacitation of multiple critical sensor nodes on wireless sensor network lifetime, IEEE Wireless Commun. Lett. 6 (3) (2017) 306–309.

[32] Z. Fei, B. Li, S. Yang, C. Xing, H. Chen, L. Hanzo, A survey of multiobjective optimization in wireless sensor networks: Metrics, algorithms, and open problems, IEEE Commun. Surveys Tuts. 19 (1) (2017) 550–586.

[33] S. Kurt, B. Tavli, Path loss modeling for wireless sensor networks: A review of models and comparative evaluations, IEEE Antennas Propag. Mag. 59 (1) (2017) 18–37.

[34] Tmote Sky Datasheet, `https://usermanual.wiki/Sentilla/TMOTESKY`, accessed: 2021-01-24 (2021).

[35] S. R. Shanmugham, S. Paramasivam, Survey on power analysis attacks and its impact on intelligent sensor networks, IET Wireless Sensor Syst. 8 (6) (2018) 295–304.

[36] I. Jawhar, N. Mohamed, K. Shuaib, A framework for pipeline infrastructure monitoring using wireless sensor network, in: Proc. Ann. Wireless Telecommun. Symp. (WTS), 2007, pp. 1–7.

[37] I. Jawhar, N. Mohamed, A hierarchical and topological classification of linear sensor networks, in: Proc. Wireless Telecommun. Symp. (WTS), 2009, pp. 1–8.

[38] I. Stoianov, L. Nachman, S. Madden, T. Tokmouline, PIPENET: A wireless sensor network for pipeline monitoring, in: Proc. Int. Symp. Informat. Process. Sensor Netw. (IPSN), 2007, pp. 264–273.

[39] M. Zimmerling, W. Dargie, J. M. Reason, Energy-efficient routing in linear wireless sensor networks, in: Proc. IEEE Int. Conf. Mobile Adhoc Sensor Syst. (MOBIHOC), 2007, pp. 1–3.

[40] A. Hossain, T. Radhika, S. Chakrabarti, P. K. Biswas, An approach to increase the lifetime of a linear array of wireless sensor nodes, Int. J. Wireless Inf. Netw. 15 (2) (2008) 72–81.

[41] M. Noori, M. Ardakani, Characterizing the traffic distribution in linear wireless sensor networks, IEEE Comm. Lett. 12 (8) (2008) 554–556.

[42] S. Yoon, W. Ye, J. Heidemann, B. Littlefield, C. Shahabi, SWATS: Wireless sensor networks for steamflood and waterflood pipeline monitoring, IEEE Netw. 25 (1) (2011) 50–56.

[43] B. Wan, W. Zhang, The lifetime optimization strategy of linear random wireless sensor networks based on mobile sink, in: Proc. Int. Conf. Wireless Commun. Sensor Netw. (WCSN), 2014, pp. 258–261.

[44] S. Ali, A. Ashraf, S. B. Qaisar, M. Kamran Afridi, H. Saeed, S. Rashid, E. A. Felemban, A. A. Sheikh, SimpliMote: A wireless sensor network monitoring platform for oil and gas pipelines, IEEE Syst. J. 12 (1) (2018) 778–789.

[45] A. Kara, M. A. Al Imran, K. Karadag, Linear wireless sensor networks for cathodic protection monitoring of pipelines, in: Proc. Int. Conf. Mechat. Robot. Syst. Eng. (MoRSE), 2019, pp. 233–236.

[46] F. Tong, S. He, J. Pan, Modeling and analysis for data collection in duty-cycled linear sensor networks with pipelined-forwarding feature, IEEE Internet Things J. 6 (6) (2019) 9489–9502.

[47] S. Khoshabi Nobar, F. Mansourkiaie, M. H. Ahmed, Packet dropping minimization in energy harvesting-based wireless sensor network with linear topology, IEEE Access 8 (2020) 38682–38691.

[48] O. Flauzac, J. Herard, F. Nolot, Synchronization solution to optimize power consumption in linear sensor network, in: Proc. Int. Conf. Fog Mobile Edge Comput. (FMEC), 2020, pp. 295–300.

[49] A. Hussein, A. Elnakib, S. Kishk, Linear wireless sensor networks energy minimization using optimal placement strategies of nodes, Wireless Pers. Commun. 114 (2020) 2841–2854.

[50] B. Nemade, D. Shah, IoT based water parameter testing in linear topology, in: Proc. Int. Conf. Cloud Comput. Data Sci. Eng. (Confluence), 2020, pp. 546–551.

[51] S. Bin, G. Sun, Optimal energy resources allocation method of wireless sensor networks for intelligent railway systems, Sensors 20 (2) (2020) 482:1–482:20.

[52] S. Varshney, C. Kumar, A. Swaroop, Lightning-based lion optimization algorithm for monitoring the pipelines using linear wireless sensor network, Wireless Pers. Commun. 20 (Nov. 2020).

[53] M. A. A. Imran, Y. Dalveren, B. Tavli, A. Kara, Optimal operation mode selection for energy-efficient light-weight multi-hop time synchronization in linear wireless sensor networks, EURASIP J. Wireless Commun. Netw. (2020) 109:1–109:9.

[54] C. E. Acosta, F. Gil-Castieira, C. E. Gualotua, Optimization of delays and power consumption in large-scale linear networks using iACK, in: Proc. IEEE Andean Conf. (ANDESCON), 2020, pp. 1–5.

[55] S. Tabatabaei, A novel fault tolerance energy-aware clustering method via social spider optimization (SSO) and fuzzy logic and mobile sink in wireless sensor networks (WSNs), Comput. Syst. Sci. Eng. 35 (6) (2020) 477–494.

[56] N. Mohamed, J. Al-Jaroodi, I. Jawhar, Modeling the performance of faulty linear wireless sensor networks, Int. J. Distrib. Sens. Netw. 10 (7) (2014) 835473:1–835473:12.

[57] N. Wang, Y. Fu, J. Zhao, L. Chen, Node importance measure in linear wireless sensor networks, Adv. Mech. Eng. 8 (12) (2016) 1–7.

[58] Y. Mo, Efficient analysis of hybrid LWSN for the linear infrastructure monitoring, in: Proc. Int. Conf. Sens. Diagn. Prognostics Control (SDPC), 2017, pp. 518–523.

[59] Y. Mo, L. Xing, J. Jiang, Modeling and analyzing linear wireless sensor networks with backbone support, IEEE Trans Syst., Man, Cybern. Syst. 50 (10) (2020) 3912–3924.

[60] A. Tommaso, F. Ada, L. Elia, M. Marco, P. Enza, P. Alessandro, V. Valerio, Reliability and availability evaluation of linear LoRaWAN sensor network architectures for pipeline monitoring, in: Proc. IEEE Int. Instrument. Measurem. Techn. Conf. (I2MTC), 2020, pp. 1–6.

[61] E. Y. Vasserman, N. Hopper, Vampire attacks: Draining life from wireless ad hoc sensor networks, IEEE Trans. Mobile Comput. 12 (2) (2013) 318–332.

[62] V. Shakhov, On a new type of attack in wireless sensor networks: Depletion of battery, in: Proc. Int. Forum Strat. Tech. (IFOST), 2016, pp. 491–494.

[63] R. Nawal, R. Kaur, Abnormal leakage of energy in battery-based IoT-devices, in: Proc. Int. Conf. Secur. Informat. Netw. (SIN), 2017, pp. 165–170.

[64] E. Gelenbe, Y. M. Kadioglu, Energy life-time of wireless nodes with network attacks and mitigation, in: Proc. IEEE Int. Conf. Commun. Workshops (ICC Workshops), 2018, pp. 1–6.

[65] U. Ashraf, PROSE-proactive resilience in internet of things: Targeted attacks and countermeasures, IEEE Sensors J. 18 (24) (2018) 10049–10057.

[66] G. S. Dhunna, I. Al-Anbagi, A low power wsns attack detection and isolation mechanism for critical smart grid applications, IEEE Sensors J. 19 (13) (2019) 5315–5324.

[67] A. Gallais, T. Hedli, V. Loscri, N. Mitton, Denial-of-sleep attacks against IoT networks, in: Proc. Int. Conf. Control Decision Informat. Tech. (CoDIT), 2019, pp. 1025–1030.

[68] V. Nguyen, P. Lin, R. Hwang, Energy depletion attacks in low power wireless networks, IEEE Access 7 (2019) 51915–51932.

[69] S.-Y. Chang, S. L. S. Kumar, Y.-C. Hu, Y. Park, Power-positive networking: Wireless-charging-based networking to protect energy against battery DoS attacks, ACM Trans. Sens. Netw. 15 (3) (2019) 27:11–27:25.

[70] S. Xiang, J. Yang, Reliability evaluation and reliability-based optimal design for wireless sensor networks, IEEE Syst. J. 14 (2) (2020) 1752–1763.

[71] S. Lin, F. Miao, J. Zhang, G. Zhou, L. Gu, T. He, J. A. Stankovic, S. Son, G. J. Pappas, ATPC: Adaptive transmission power control for wireless sensor networks, ACM Trans. Sens. Netw. 12 (1) (2016) 6:1–6:31.

[72] O. Cayirpunar, B. Tavli, E. Kadioglu-Urtis, S. Uludag, Optimal mobility patterns of multiple base stations for wireless sensor network lifetime maximization, IEEE Sensors J. 17 (21) (2017) 7177–7188.

[73] M. Elwekeil, M. S. Abdalzaher, K. Seddik, Prolonging smart grid network lifetime through optimising number of sensor nodes and packet length, IET Commun. 13 (16) (2019) 2478–2484.

[74] V. Freschi, E. Lattanzi, A study on the impact of packet length on communication in low power wireless sensor networks under interference, IEEE Internet Things J. 6 (2) (2019) 3820–3830.

[75] H. Cui, B. Zhang, Y. Yan, C. Li, Optimal packet size analysis for network coding-enabled two-hop error-prone wireless networks, IEEE Commun. Lett. 23 (5) (2019) 904–908.

[76] H. Cheng, C. Wang, X. Zhang, An opportunistic routing in energy-harvesting wireless sensor networks with dynamic transmission power, IEEE Access 7 (2019) 180652–180660.

[77] A. Pal, A. Nasipuri, Joint power control and routing for rechargeable wireless sensor networks, IEEE Access 7 (2019) 123992–124007.

[78] M.A.Daz-Ibarra, D.U.Campos-Delgado, C.A.Gutirrez, J.M.Luna-Rivera, Distributed power control in mobile wireless sensor networks, Ad Hoc Netw. 85 (2019) 110–119.

[79] D. Mu, Y. Ge, M. Sha, S. Paul, N. Ravichandra, S. Chowdhury, Robust optimal selection of radio type and transmission power for internet of things, ACM Trans. Sens. Netw. 15 (4) (2019) 39:1–39:25.

[80] E. Lattanzi, P. Capellacci, V. Freschi, Experimental evaluation of the impact of packet length on wireless sensor networks subject to interference, Comput. Netw. 167 (2020) 106986:1–106986:12.

[81] A. S. A. Azman, M. Y. Lee, S. K. Subramaniam, F. S. Feroz, Performance evaluation of grid wireless sensor network with different packet size for pipeline in downstream of oil and gas industry, IOP Conf. Ser. Mater. Sci. Eng. 765 (2020) 1–9.

[82] H.-S. Kim, J. Paek, D. E. Culler, S. Bahk, PC-RPL: Joint control of routing topology and transmission power in real low-power and lossy networks, ACM Trans. Sens. Netw. 16 (2) (2020) 14:1–14:31.

[83] N. Zogovic, Energy efficiency versus reliability tradeoff improvement in low-power wireless communications, IEEE Syst. J. 14 (3) (2020) 3173–3184.

[84] H. Cotuk, B. Tavli, K. Bicakci, M. B. Akgun, The impact of bandwidth constraints on the energy consumption of wireless sensor networks, in: Proc. IEEE Wireless Commun. Netw. Conf. (WCNC), 2014, pp. 2787–2792.

[85] V. K. Akram, O. Dagdeviren, B. Tavli, Distributed k-connectivity restoration for fault tolerant wireless sensor and actuator networks: Algorithm design and experimental evaluations, IEEE Trans. Rel. 70 (3) (2021) 1112–1125.

[86] O. Dagdeviren, V. K. Akram, B. Tavli, Design and evaluation of algorithms for energy efficient and complete determination of critical nodes for wireless sensor network reliability, IEEE Trans. Rel. 68 (1) (2019) 280–290.

[87] K. Akkaya, F. Senel, A. Thimmapuram, S. Uludag, Distributed recovery from network partitioning in movable sensor/actor networks via controlled mobility, IEEE Trans. Comput. 59 (2) (2010) 258–271.

[88] GAMS Development Corporation, General Algebraic Modeling System (GAMS) Release 25.0.3, Washington, DC, USA (2018).
URL http://www.gams.com/